Supporting Information

Sustainable Solar Seawater Splitting over a $BaTaO_2N$ Photoanode Enabled by Chloride Recirculation

Jeongsuk Seo*, Seongeon Mun, Van-Huy Trinh

Department of Chemistry, College of Natural Sciences, Chonnam National University, 77 Yongbong-ro, Buk-gu, Gwangju 61186, Republic of Korea

*Corresponding author: *j_seo@chonnam.ac.kr*

Keywords: Solar Seawater Splitting, Hydrogen Production, Perovskite Oxynitrides, Chlorine Evolution Reaction, Chloride Regeneration

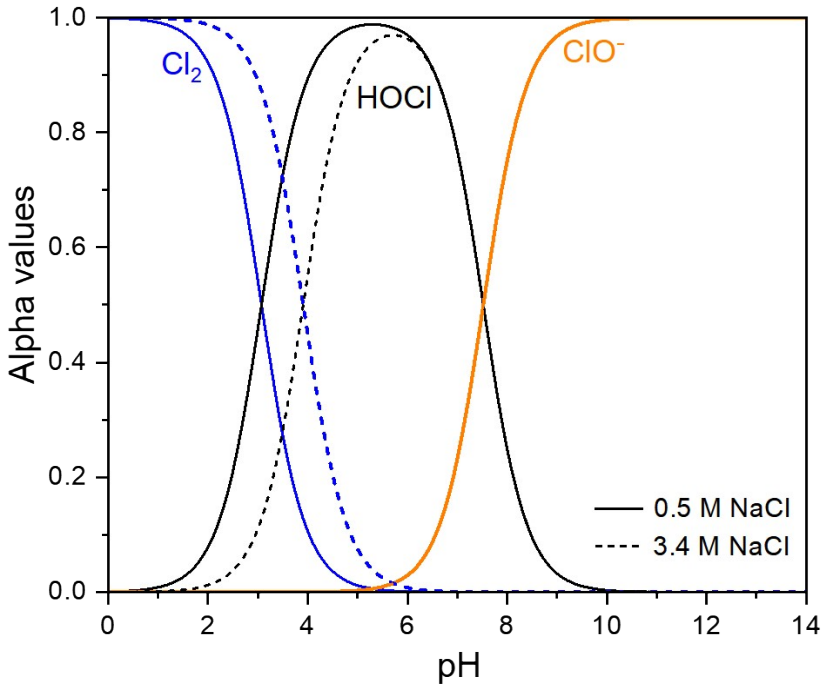

Figure S1. Alpha values of free chlorine species, i.e., Cl_2, HOCl, and ClO^-, as a function of pH values in aqueous 0.5 and 3.4 M NaCl solutions. The fractions are computed from chemical equilibria (equation 3 and 4) for Cl_2 hydrolysis and dissociation of HOCl acid.

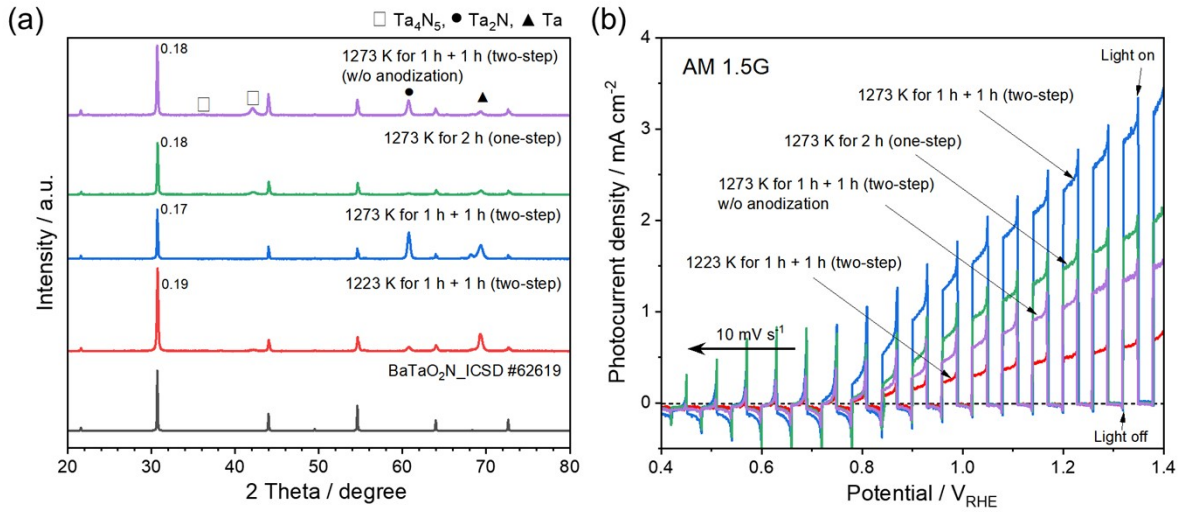

Figure S2. (a) XRD patterns for the $BaTaO_2N$/Ta photoanodes synthesized through one- and two-step nitridation at 1223 and 1273 K for total 2 h with and without anodization of Ta substrate. (b) LSV data for corresponding $Co(OH)_x$/$BaTaO_2N$/Ta photoanodes during seawater splitting at pH 6.4 under chopped AM 1.5G simulated sunlight. All photoelectrochemical data were acquired by sweeping the potential from 1.4 to 0.4 V_{RHE} at a scan rate of 10 mV s^{-1} in an Ar-saturated 0.5 M NaCl aqueous electrolyte buffered with 0.2 M KPi.

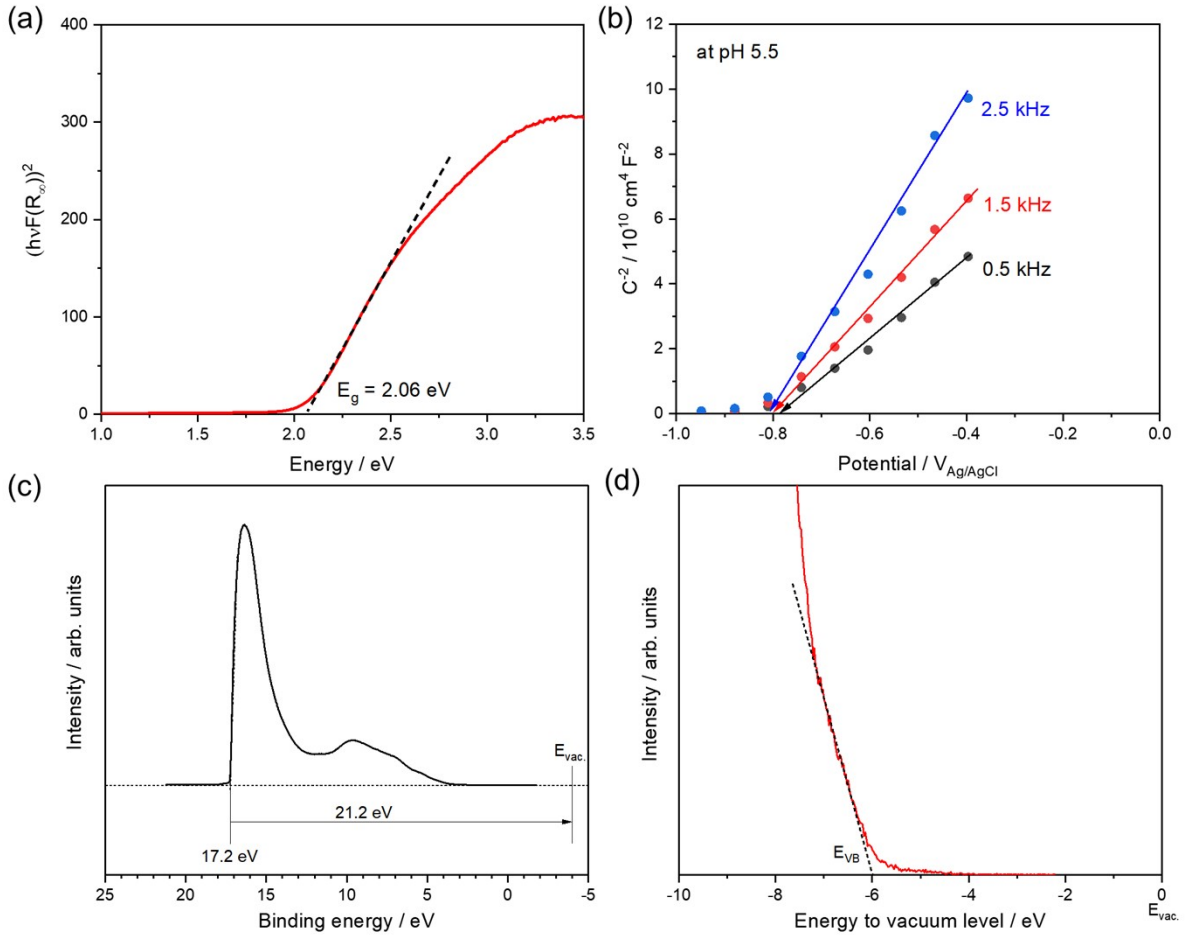

Figure S3. (a) A Tauc plot of $BaTaO_2N$ grown on quartz glass for a direct allowed transition. The Tauc plot was derived from its UV–Vis DRS spectrum using the relation, $\alpha h\nu = A(h\nu - E_g)^{n/2}$, where α is the absorption coefficient, h is Planck's constant, ν is the photon frequency, A is a proportionality factor, and n is an exponent that characterizes the type of optical transition in the semiconductor (n = 1 for a direct allowed transition). The intercept on the x-axis corresponds to E_g of $BaTaO_2N$. (b) Mott-Schottky (MS) plots for bare $BaTaO_2N$/Ta photoanodes prepared by bottom-up fabrication. The measurements were performed in an Ar-saturated 0.5 M NaCl electrolyte buffered with 0.2 M KPi at pH 5.5 under dark conditions with an AC amplitude of 15 mV at different frequencies of 0.5, 1.5, and 2.5 kHz. The MS plots were analyzed based on the relation $1/C^2 = 2/(\varepsilon\varepsilon_0 e N_D)(E - E_{fb})$, where C is the space-charge capacitance, ε is the dielectric constant of the semiconductor, ε_0 is the vacuum permittivity, e is the elementary charge, N_D is the donor density, E is the applied potential, and E_{fb} is the flat-band potential. The intercept on the x-axis indicates E_{fb} of $BaTaO_2N$. (c) A UPS spectrum of bare $BaTaO_2N$/Ta photoanode obtained using E_B (vs. Fermi) + E_K + $\Phi_{analyzer}$ = 21.2 eV (see the Experimental Section) and (d) its corresponding spectrum with respect to the vacuum level in the valence band region, transformed by E_B (vs. vacuum) = $-(\Phi_{semiconductor} + E_B$ (vs. Fermi)). The work function of the semiconductor was calculated as $\Phi_{semiconductor}$ = 21.2 eV − E_{cutoff} (17.2 eV). E_{VB} and conduction band minimum potentail, E_{CB}, of the $BaTaO_2N$/Ta photoanode were determined by linear extrapolation of the spectrum in the valence band region and from the relation $E_{CB} = E_{VB} + E_g$, respectively.

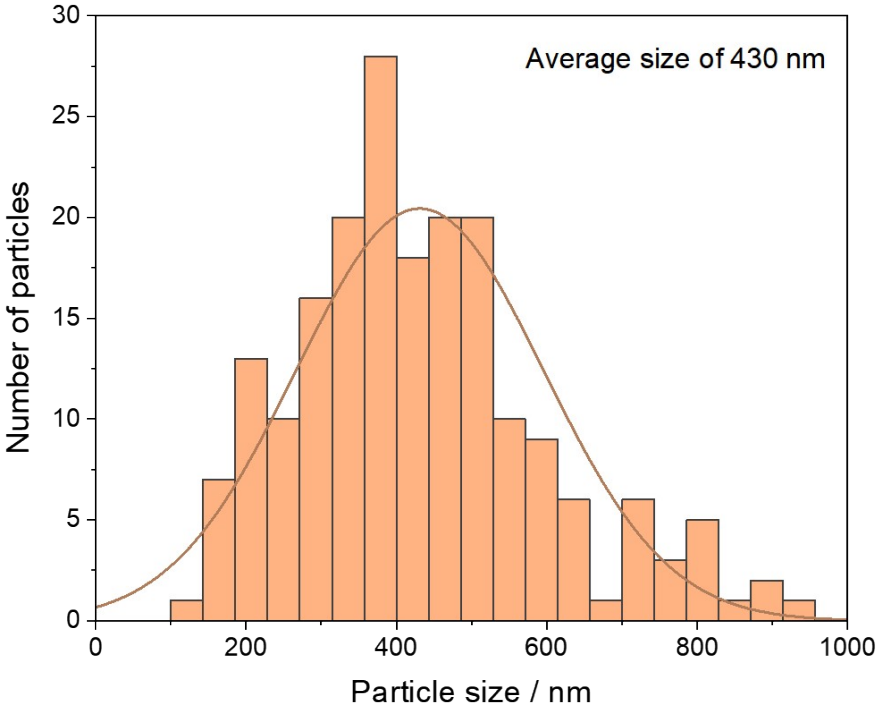

Figure S4. Size distribution of cuboidal $BaTaO_2N$ particles grown on a Ta substrate prepared via bottom-up fabrication.

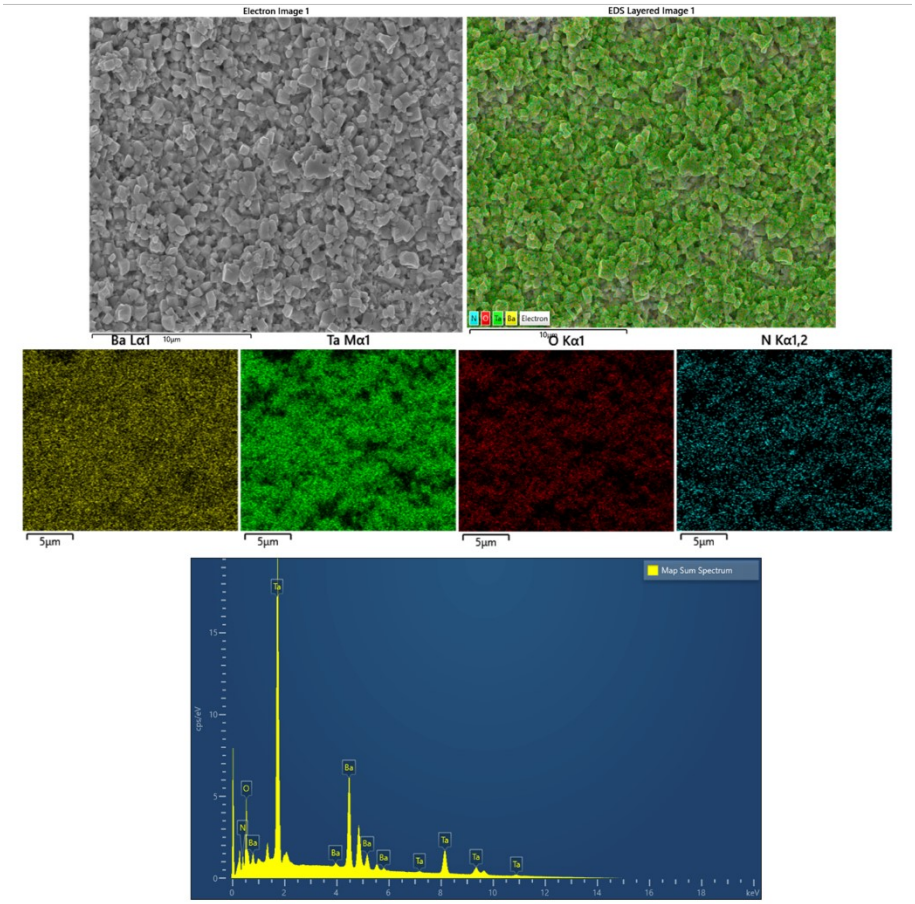

Region	Ba(%)	Ta(%)	Ba/Ta	O(%)	N(%)	O/N
1	24.7	21.5	1.2	34.8	19.1	1.8
2	24.0	21.2	1.1	35.0	19.9	1.8
3	24.0	21.4	1.1	34.7	20.0	1.7
Mean			1.1			1.8

Figure S5. Elemental EDS mapping of the prepared $BaTaO_2N$/Ta photoanode and corresponding surface elemental atomic ratios (Ba/Ta and O/N) measured at three distinct regions.

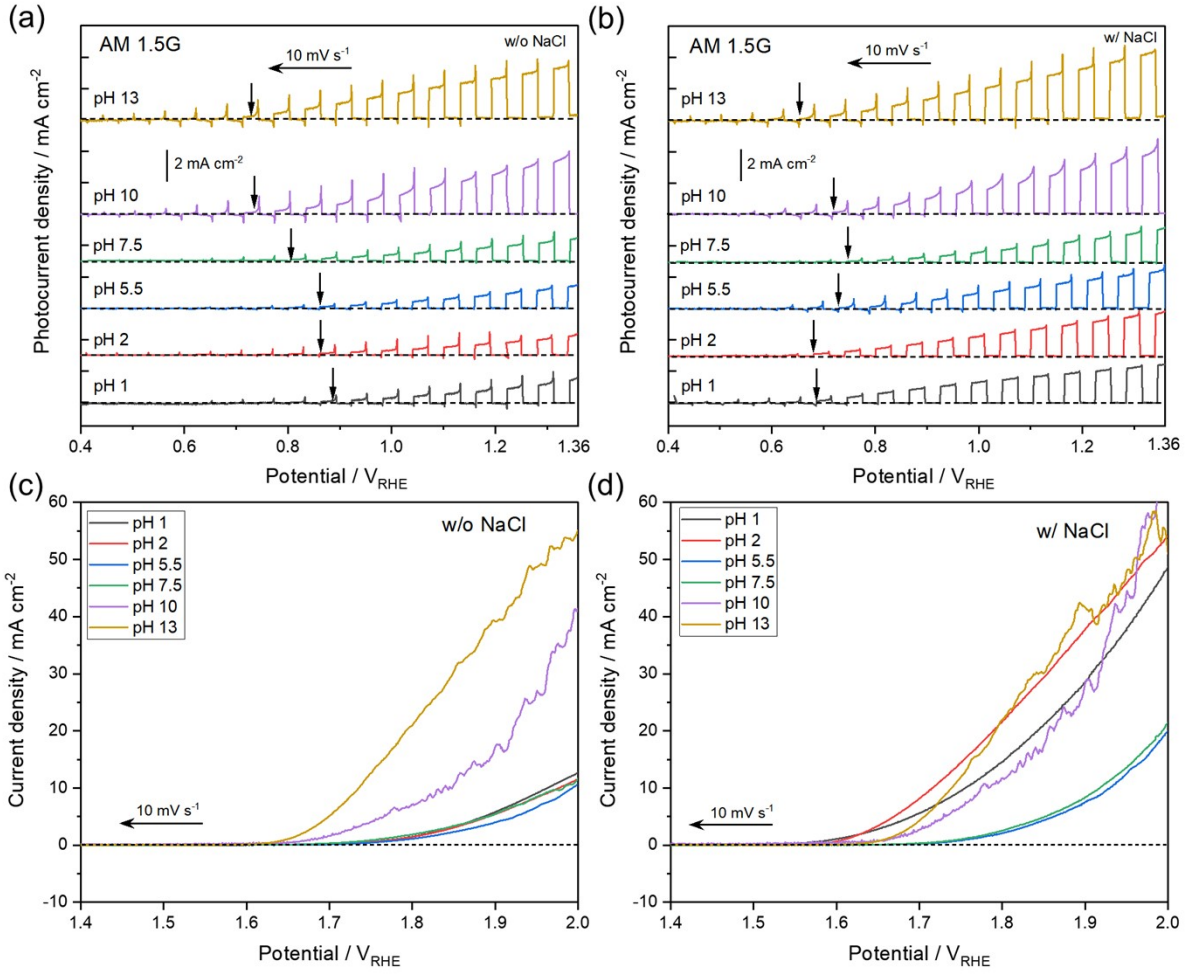

Figure S6. (a, b) LSV data for $Co(OH)_x/BaTaO_2N/Ta$ photoanodes during (a) water splitting and (b) seawater splitting at different pH under chopped AM 1.5G simulated sunlight. All photoelectrochemical data were acquired by sweeping the potential from 1.36 to 0.4 V_{RHE} at a scan rate of 10 mV s^{-1} in an Ar-saturated 0.2 M KPi aqueous electrolyte. 0.5 M NaCl was dissolved in the electrolyte for seawater splitting. (c, d) LSV data for $Co(OH)_x$/FTO electrodes during (c) water splitting and (d) seawater splitting at different pH in darkness. The electrochemical data were recorded by scanning the potential from 2.0 to 1.4 V_{RHE} at a scan rate of 10 mV s^{-1} in an Ar-saturated 0.2 M KPi aqueous electrolyte. 0.5 M NaCl was dissolved in the electrolyte for seawater splitting.

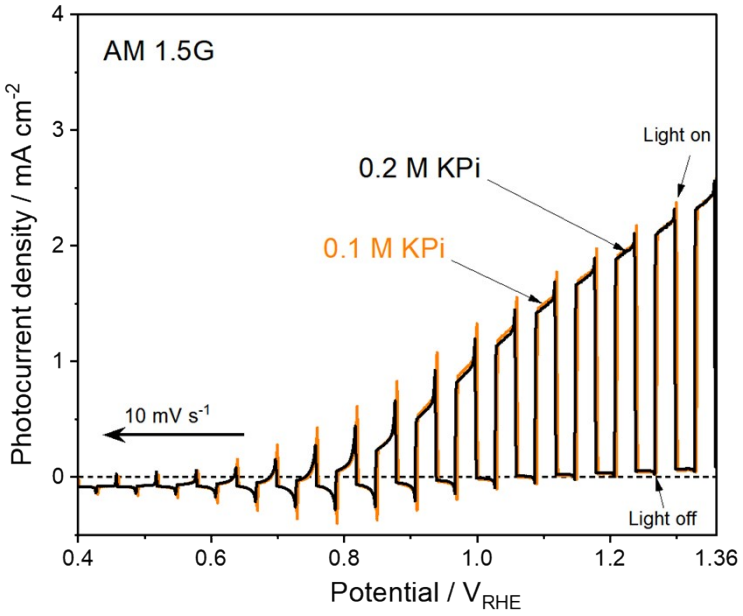

Figure S7. LSV data for a $Co(OH)_x/BaTaO_2N/Ta$ photoanode during seawater splitting in a 0.5 M NaCl aqueous electrolyte buffered with 0.1 and 0.2 M KPi under chopped AM 1.5 G sunlight.

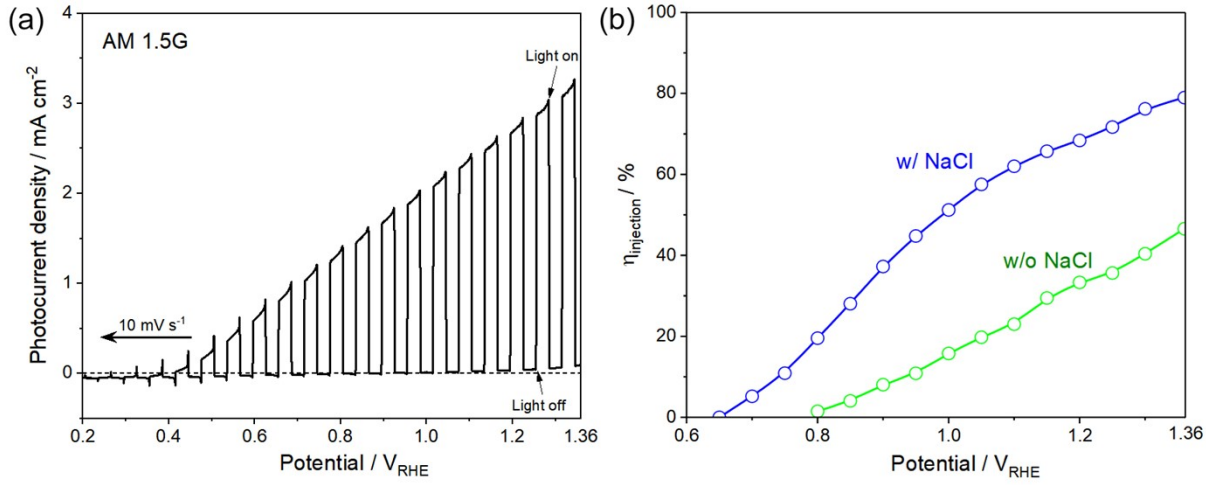

Figure S8. (a) LSV data for a $Co(OH)_x/BaTaO_2N/Ta$ photoanode during sulfite oxidation in a 0.5 M Na_2SO_3 aqueous electrolyte buffered with 0.2 M KPi under chopped AM 1.5 G sunlight. (b) Charge injection efficiencies, η_{inj} (%), of the corresponding photoanode for seawater (w/ NaCl) and water splitting (w/o NaCl). The efficiencies were quantified from LSV curves presented in Figure 3(c) according to the relation, η_{inj} (%) = $J_{w/\ NaCl\ or\ w/o\ NaCl}$ (V)/J_{Na2SO3}(V) × 100.

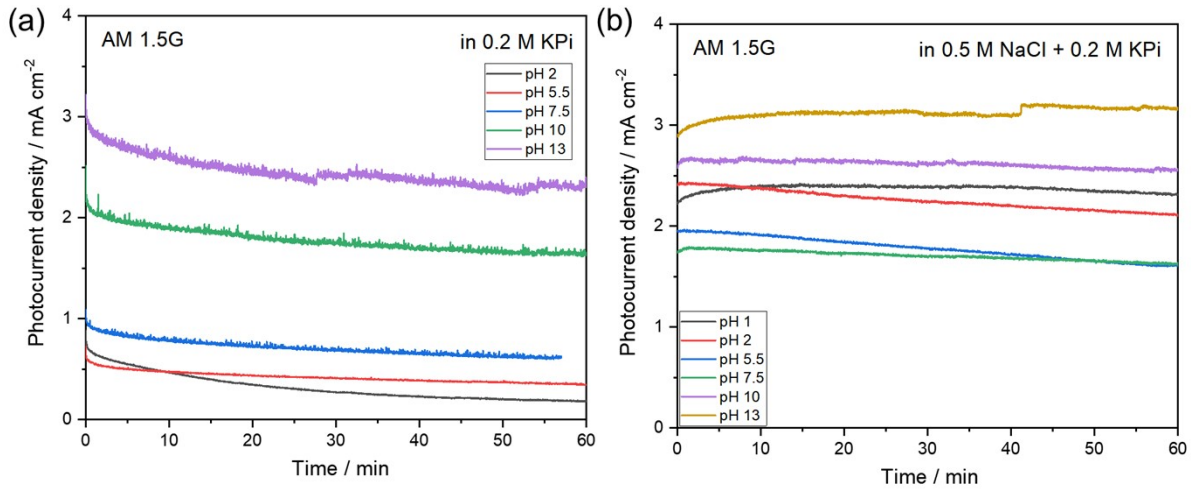

Figure S9. Chronoamperometry curves acquired using $Co(OH)_x/BaTaO_2N/Ta$ photoanodes during seawater splitting at an applied potential of 1.23 V_{RHE} for 1 h under chopped AM 1.5 G simulated sunlight in stirred Ar-saturated 0.2 M KPi aqueous electrolytes dissolved without (a) and with 0.5 M NaCl (b) at different pH values.

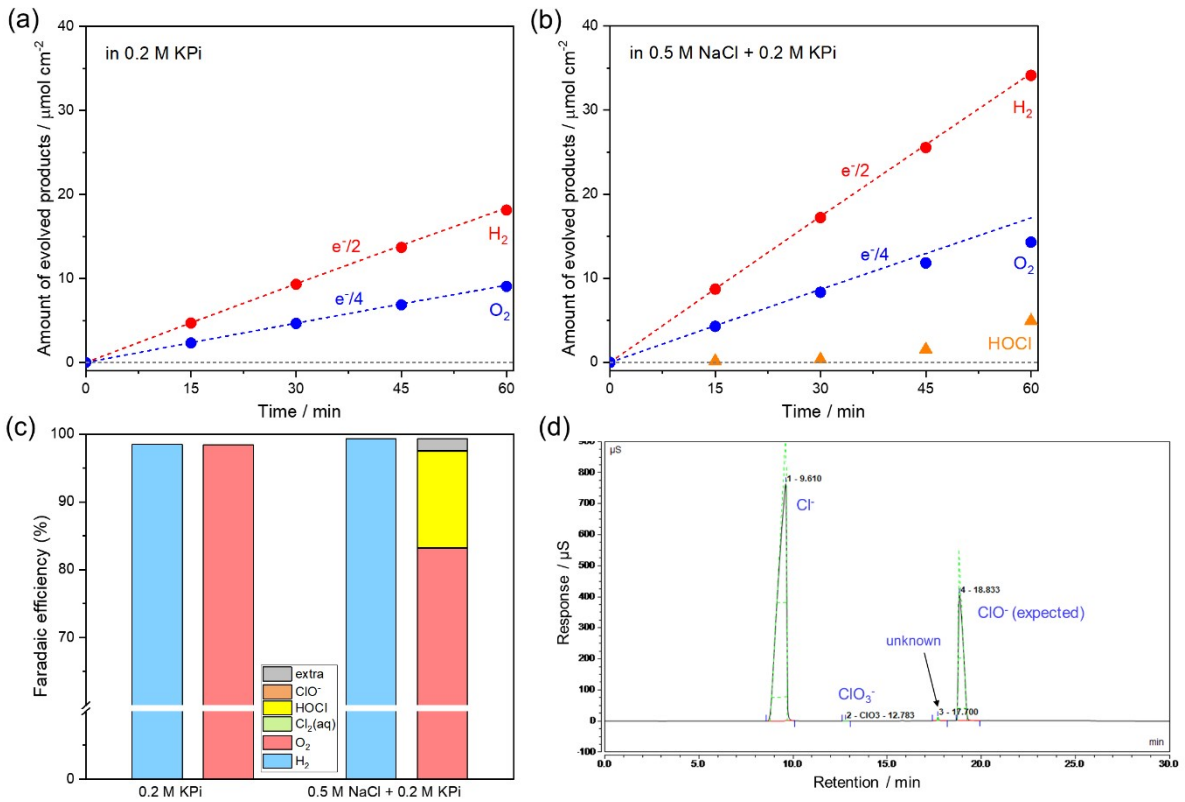

Figure S10. Time courses of O_2 and free chlorine (HOCl), H_2 generation over the $Co(OH)_x/BaTaO_2N/Ta$ photoanode, and a Pt wire during (a) water splitting and (b) seawater splitting at the applied potential of 1.23 V_{RHE} under AM 1.5G simulated sunlight in Ar-saturated aqueous 0.2 M KPi electrolytes adjusted to pH 5.5. 0.5 M NaCl was dissolved in the electrolyte for seawater splitting. The dashed lines indicate the amounts of H_2, HOCl ($e^-/2$), and O_2 ($e^-/4$) expected for a Faradaic efficiency of unity. (c) A bar chart for Faradaic efficiencies estimated by quantitative analyses of products shown in (a) and (b). (d) An ion chromatogram in an alkalline environmnet showing Cl^-, ClO_3^-, and ClO^- species in the electrolyte after solar seawater splitting for 1 h shown in (b).

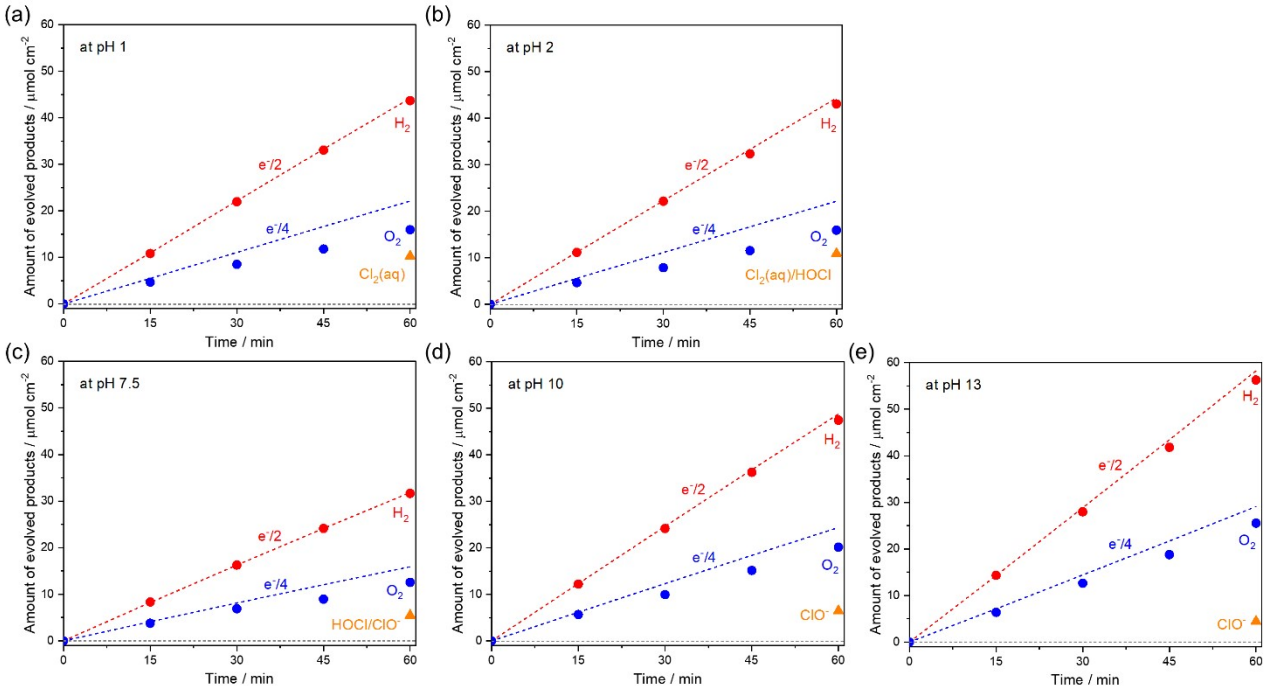

Figure S11. Time courses of O_2 and free chlorine (HOCl), H_2 generation over the $Co(OH)_x/BaTaO_2N/Ta$ photoanodes, and Pt wires during seawater splitting at the applied potential of 1.23 V_{RHE} under AM 1.5G simulated sunlight in Ar-saturated aqueous 0.5 M NaCl electrolytes buffered with 0.2 M KPi and adjusted to different pH values of (a) 1, (b) 2, (c) 7.5, (d) 10, and (e) 13. The dashed lines indicate the amounts of H_2, free chlorine ($Cl_2(aq)/HOCl/ClO^-$) ($e^-/2$), and O_2 ($e^-/4$) expected for a Faradaic efficiency of unity.

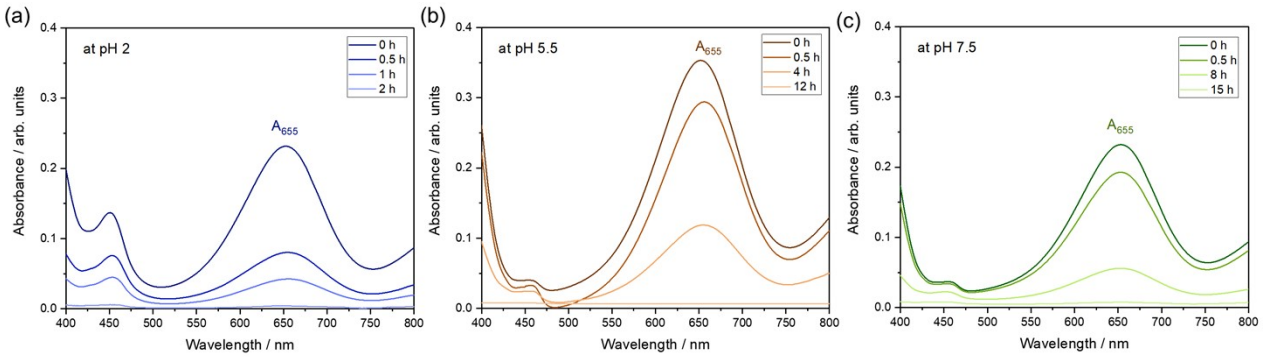

Figure S12. UV-vis absorption spectra of the TMB solutions in the presence of different concentrations of free chlorine during the decomposition of free chlorine species in aqueous 2.7 μM NaOCl electrolytes buffered with 0.2 M KPi adjusted to different pH of (a) 2, (b) 5.5, and (c) 7.5 under AM 1.5G simulated sunlight irradiation, shown in Figure 4(a). Since the absorbance of oxidized TMB at 655 nm is pH-dependent, the concentration of free chlorine was calibrated separately for each pH. A gradual decrease in A_{655} over time was observed, indicating the progressive decomposition of free chlorine and the corresponding decline in its concentration.

Table S1. Summary of reported $BaTaO_2N$ photoanodes prepared by different synthesis routes and their photoelectrochemical activity and long-term stability, compared with the present work.

Year	Photoanode	Synthesis	Photocurrent density	Retention	Reference
2025	$Co(OH)_x/BaTaO_2N/Ta$	Bottom-up fabrication	2 mA cm^{-2} at 1.23 V_{RHE} in 0.5 M NaCl (pH 5.5)	81% for 24 h	This work
2015	$Co/BaTaO_2N/Ta/Ti$	Particle transfer	4.2 mA cm^{-2} at 1.20 V_{RHE} in 0.5 M KPi (pH 13)	80% for 6 h	J. Am. Chem. Soc. 137 (2015) 2227
2016	$CoPi/BaTaO_2N/Ta$	Hydrothermal method	0.75 mA cm^{-2} at 1.23 V_{RHE} in 0.5 M KPi (pH 13)	97% for 5 h	J. Phys. Chem. C 120 (2016) 15758.
2019	$Co(OH)_x$-$FeO_y/BaTaO_2N/Ti$	Particle transfer	6.5 mA cm^{-2} at 1.23 V_{RHE} in 0.5 M KBi (pH 13)	79% for 24 h	ACS Appl. Energy Mater., 2(8), (2018) 5777.
2019	$CoO_x/BaTaO_2N/Ta/Ti$	Particle transfer	3.11 mA cm^{-2} at 1.20 V_{RHE} in 0.2 M KPi (pH 13)	-	Faraday Discuss., 215, (2019) 227
2020	$CoO_x/BaTaO_2N/Ta_2N/Ta$	Interfacial reaction	4.6 mA cm^{-2} at 1.23 V_{RHE} in 0.1 M KPi (pH 13)	65% for 3 h	Solar RRL 4, (2020) 1900542.
2020	$CoO_x/BaTaO_2N/FTO$	Electrophoretic deposition	2.05 mA cm^{-2} at 1.23 V_{RHE} in 0.1 M KOH (pH = 13)	94% for 1 h	Chem. Comm., 57, (2021) 4412
2022	$NiCoFe\text{-}B_i/BaTaO_2N/Nb$	Dual-source electron beam deposition	4.7 mA cm^{-2} at 1.23 V_{RHE} in 1 M KOH (pH = 13.6)	78.5% for 13.3 h	J. Catal., 411, (2022) 109

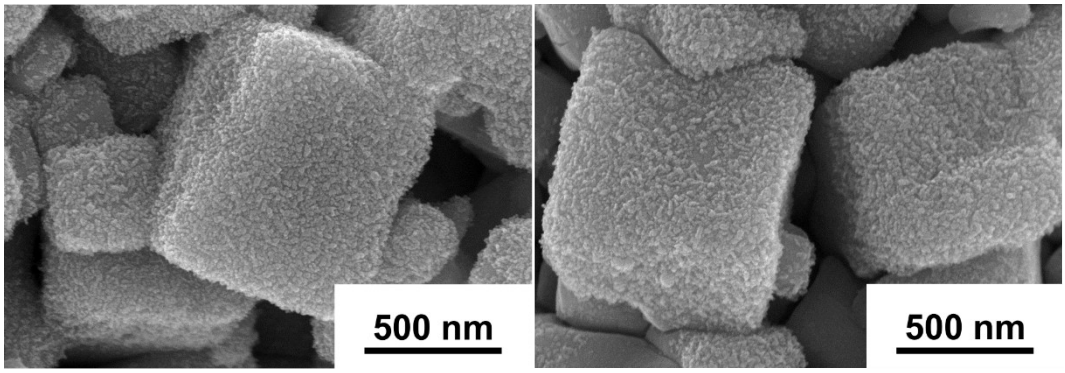

Figure S13. Top-view SEM images of $Co(OH)_x/BaTaO_2N/Ta$ photoanodes after long term seawater splitting for 24 h at an applied potential of 1.23 V_{RHE} under chopped AM 1.5 G simulated sunlight in stirred Ar-saturated 0.5 M NaCl electrolyte buffered with 0.2 M KPi and adjusted to pH 5.5.